RILEM Bookseries

Savvas Saloustros
Katrin Beyer *Editors*

Structural Analysis of Historical Constructions

SAHC 2025, Volume 1

Springer

RILEM Bookseries

Volume 64

RILEM, The International Union of Laboratories and Experts in Construction Materials, Systems and Structures, founded in 1947, is a non-governmental scientific association whose goal is to contribute to progress in the construction sciences, techniques and industries, essentially by means of the communication it fosters between research and practice. RILEM's focus is on construction materials and their use in building and civil engineering structures, covering all phases of the building process from manufacture to use and recycling of materials. More information on RILEM and its previous publications can be found on www.RILEM.net.

Indexed in SCOPUS, Google Scholar and SpringerLink.

Savvas Saloustros · Katrin Beyer
Editors

Structural Analysis of Historical Constructions

SAHC 2025, Volume 1

Springer

Editors
Savvas Saloustros
ENAC IIC EESD
EPFL
Lausanne, Switzerland

Katrin Beyer
ENAC IIC EESD
EPFL
Lausanne, Switzerland

ISSN 2211-0844 ISSN 2211-0852 (electronic)
RILEM Bookseries
ISBN 978-3-032-13468-4 ISBN 978-3-032-13469-1 (eBook)
https://doi.org/10.1007/978-3-032-13469-1

This Springer imprint is published by the registered company Springer Nature Switzerland AG
The registered company address is: Gewerbestrasse 11, 6330 Cham, Switzerland

Laboratory Tests for the Characterisation of a Sedimentary Arenaceous Limestone Used in the Architectural Heritage of Northern Italy

Giuliana Cardani[1], Michela Rossi[2(✉)], and Dionysios Bournas[2]

[1] Politecnico di Milano, 20133 Milan, Italy
[2] European Commission, Joint Research Centre (JRC), 21027 Ispra, Italy
michela.rossi@ec.europa.eu

Abstract. The Saltrio stone, a clastic sedimentary rock from the Italy-Swiss border, has been used in Northern Italy's architectural heritage since the 15th century, with notable examples including the Santa Maria delle Grazie church in Milan and the Certosa di Pavia. Despite its historical relevance, the extraction of Saltrio stone has shifted from sourcing whole blocks for construction to producing only crushed aggregate, limiting its potential and supply for the preservation and rehabilitation of heritage buildings. To ensure the successful preservation interventions of so many cultural assets, it is essential to conduct physical and mechanical characterisation of this stone. A laboratory test campaign was conducted to gather information on the chemical, physical, and mechanical properties of the stone material. The results will provide valuable information not only for cultural heritage conservation, given the lack of such characterisation in existing literature, but also for assessing the structural capacity of existing heritage structures. Furthermore, they will support more accurate predictions before and during experimental tests on full-scale historical buildings in laboratory settings.

Keywords: Laboratory tests · Sedimentary stone · Limestone · Mechanical parameters · Laboratory characterization · Cultural Heritage

1 Introduction

Stone has been used in Italian architecture since ancient times, especially in northern Italy, close to the Alps. Stones of high and low quality continue to enrich numerous buildings, from the simplest of rural architecture to noble palaces and religious buildings and monuments. Among these stones, the Saltrio stone is analysed, a sedimentary limestone from the Varese area that, although little known, has been used for centuries in art and construction, both locally and throughout Lombardy and Switzerland. For centuries, the extraction of stone from Mount Orsa was the main source of employment and income for the local villages [1]. Currently, the quarries are in a state of neglect, are inaccessible to the public, and only one quarry remains active, from which only crushed stone is extracted.

S. Saloustros and K. Beyer (Eds.): SAHC 2025, RILEM Bookseries 64, pp. 437–450, 2026.
https://doi.org/10.1007/978-3-032-13469-1_35

This sedimentary rock is a key component of the region's architectural identity. Saltrio is located in the transnational area of the UNESCO site of Monte San Giorgio, adjacent to Lake Lugano and lies across Italian and Swiss territory. As a natural site, it showcases remarkable evidence of significant periods in the Earth's evolution and is one of the world's most important fossil-rich deposits from the Middle Triassic period.

The study of Saltrio stone is important due to its historical significance and its potential use in the conservation and structural assessment of heritage buildings. Currently, there is no comprehensive characterization of this stone in the literature, making it essential to thoroughly understand its properties for proper reuse in restoration projects. This understanding ensures that any interventions are compatible in terms of chemical, physical, and mechanical aspects, while also preserving the integrity, materiality, and historical value of cultural heritage. Additionally, characterizing the physical and mechanical behavior of Saltrio stone provides vital information for calibrating numerical models that represent masonry constructed from this stone. These models can predict the structural and seismic responses of historic masonry buildings, thereby supporting their conservation and protection.

To further investigate the behavior of this stone masonry typology, full-scale prototypes simulating historical stone masonry walls and vaults, both unreinforced and reinforced, will be constructed and tested at the European Laboratory for Structural Assessment (ELSA) of the Joint Research Centre (JRC) in Ispra, Italy. These experiments will provide valuable data for refining numerical models and enhancing the understanding of such stone masonry typologies response under seismic actions.

2 The Saltrio Stone

2.1 Geological Formation Characteristics

The Monte San Giorgio area is known for its notable natural phenomena, which have contributed to its remarkable petrographic diversity, characterized by a variety of lithotypes [2]. During the Triassic period, this area was under the sea, leading to the deposition of different marine rocks. The favourable environmental conditions persisted for approximately twelve million years, promoting the development of a rich marine fauna and facilitating the fossilisation of marine vertebrates. This resulted in the fossiliferous carbonate series of Monte San Giorgio, which includes both dolomites and limestones [3]. The geological units in this area are stacked on top of each other, tilted southward, and descend towards the Po Valley due to the processes of the Alpine orogeny (Fig. 1a).

The Saltrio stone formation dates back to the Jurassic period, specifically the Lower Lias. It primarily consists of fine, compact, and fracture-prone chipped limestones that are typically bluish-gray or hazel in color. Many of these stones display mottling that ranges from purplish-red to pinkish-red. The formation features plane-parallel layering, with thicknesses varying between 10 and 40 cm. Saltrio stone is a sedimentary rock of biochemical origin that is calcareous, featuring calcitic cement and a compact, microcrystalline structure with fractures and microfractures. The main components include fragments of crinoid stems as well as subordinate amounts of brachiopods and mollusks. The presence of flint in the upper part of the formation indicates a transition to the overlying Moltrasio Limestone, which has been partially discarded by quarrymen because

it is unsuitable for construction and difficult to work with. For this reason, the quarries were underground and cultivation was by peculiar chambers and pillars. [4].

2.2 Saltrio Stones in Monumental and Historical Buildings

Saltrio stone has been widely used in Lombardy since the beginning of the Renaissance, spreading beyond the towns surrounding the quarries. Besides the use for masonry in the villages near the quarries, it was mainly used as decorative stone, found in features such as portals, cornices, friezes, and parapets. Saltrio stone is known for its toughness and durability; it can be cut and polished, making it ideal for constructing exterior walls and colonnades. Over time, when the stone decays, it often appears eroded, showing signs of crumbling, color changes, and the sulfate crusts formation [5].

Starting in the late 15th century, when Ludovico Sforza, the Duke of Milan, aimed to create a new architectural identity for the city, the Saltrio quarries of Monte Orsa became increasingly productive. The Renaissance, indeed, prompted a significant transformation in the Milanese buildings features, marked by a shift from brick to stone for decorative purposes. In 1497, Giovanni Antonio Amedeo - who had been the chief architect of the cathedral since 1490 and had participated in many projects of the era – used it for the Santa Maria delle Grazie church in Milan.

Saltrio stone reached its peak of use during the 17th and 18th centuries, especially for crafting ornamental elements on the façades of religious and private buildings. The neoclassical style in Milanese architecture was further developed by figures such as Piermarini, Cagnola, and Richino [6]. Some of the main monuments are: Sforza Castle, Palazzo Reale (Fig. 1b) and Vittorio Emanuele II gallery in Milan, Cathedrals of Piacenza (Fig. 1c) and of Lugano, Certosa in Pavia, Mole in Turin and others in Genova, Bergamo, Brescia and Como. The use of Saltrio stone saw a serious decline in the first half of the 20th century. This drop was due to several factors, including the rising cost of labor, which resulted in the closure of many quarries throughout Lombardy. Additionally, the increasing popularity of artificial stone and new materials contributed to its reduced usage.

(a) (b) (c)

Fig. 1. a) Saltrio stone quarry; b) View of Palazzo Reale in Milan (author Mbettacc, licensed under CC BY-SA 4.0 [7]); c) Piacenza Cathedral.

3 Physical and Mechanical Tests

3.1 Specimens Preparation

The physical and mechanical tests were carried out at the Laboratory of Material, Structure, and Construction Testing (LPMSC) of Politecnico di Milano on a series of specimens extracted from four irregular blocks samples of Saltrio stone, coming from the Salnova quarry, active since 15th century (Fig. 2a). The samples were large and quite homogeneous, making it challenging to identify the bedding planes at first glance.

After the initial cut, observations revealed that the rock was compact but not particularly hard for cutting with a water circular saw, and the bedding planes were still indistinguishable (Fig. 2b). This suggested that it falls under the category of "massive" limestones, which are characterized by a significant distance between stratification planes. Analysis of the obtained sections showed the presence of non-homogeneous inclusions and small "rust-red" spots within the rock (Fig. 2b). A bedding plane was identified through the cutting of another sample (see Fig. 3b).

Nineteen cylindrical specimens (54 mm diameter) were extracted from the stones: 13 perpendicular to the bedding plane (X direction) and 6 parallel to it (Y and Z directions), as shown in Fig. 3a. Additionally, another block was used to extract 6 prismatic specimens—3 for three-point bending and 3 for Brazilian splitting tests (Fig. 3c).

Fig. 2. a) Four Saltrio stone blocks extracted from the Salnova quarry; b) visible microfractures, inclusions, and rust-red pigmentation from a cut sample.

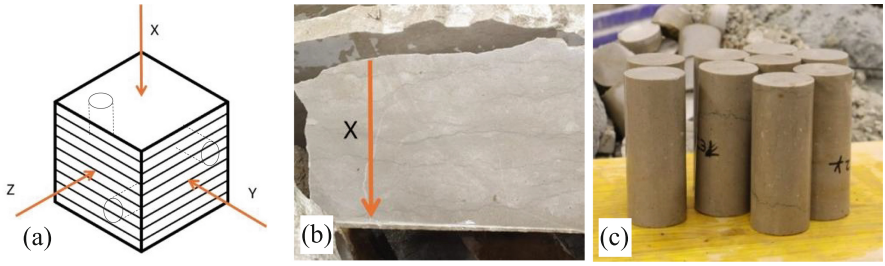

Fig. 3. a) Schematic of planar structure directions; b) bedding plane identified in a sample; c) Cylindrical specimens cored in the three planar structure directions.

3.2 Petrographic and Mineralogical Characterization

The initial phase involved visual inspections of samples, noting that characteristics vary by sampling location. The samples exhibit homogeneous greyish and yellowish hues. Under 500x optical microscopy, the limestone appears as intraclast-bioclastic with a compact, fine-grained texture containing various fossils and microfossils, cemented by calcium carbonate. In some areas, this cement extends beyond intergranular spaces, forming white spots (Fig. 4a). Additionally, blue, green, and reddish marks (Fig. 4b) indicate the presence of flint, glauconite, and iron, respectively.

These observations are more evident in polished thin sections under polarized light microscopy, where fossil microorganisms such as echinoids, lamellibranchs, sponge spicules, algae, and ostracods are clearly identified (Fig. 5a). Lithotype classification follows Dunham (1962) [8]. The fragments of Saltrio stone classify as fine-grained bioclastic Wackestone, with predominant grain sizes of 0.1–0.2 mm. The granules include Mudstone/Wackestone-type particles, echinoids, lamellibranchs, and sponge spicules with traces of flint. Porosity is minimal or absent [4].

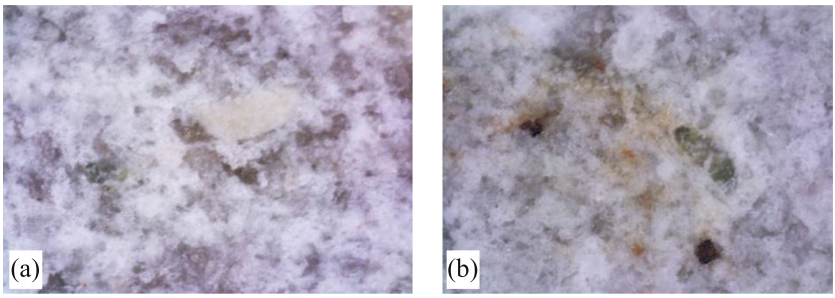

Fig. 4. 500x magnification of a sample with an optical microscope showing: (a) white spot from syntaxial cement extrusion and (b) a green inclusion and some red marks.

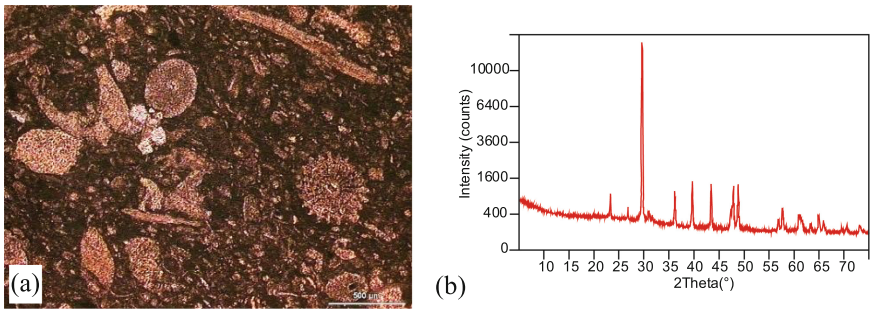

Fig. 5. (a) Micrographs of the observed thin sections under cross-polarized light evidencing different bioclasts, including echinoids and lamellibranchs; (b) Diffraction pattern showing the intensity of the diffracted X-rays as a function of the diffraction angle.

To obtain the chemical and mineralogical features at the stone's micro-scale, X-ray diffraction (XRD, Fig. 5b) and X-ray fluorescence (XRF) analyses were conducted. The analyses revealed that the Saltrio stone primarily consists of calcite, dolomite, and quartzite in varying proportions. Particularly, the XRF analyses revealed that this limestone rock is composed of calcium (Ca 29–42%), with a small percentage of magnesium (Mg 1.2–2.7%). It is interesting to note that one of the analysed samples also contains Silicium (Si 9%) and Iron (Fe 1%), distinguishing it from the others.

3.3 Physical Properties

Apparent Density and Open Porosity. The determination of apparent density (ρ_b) and open porosity (ρ_o) was conducted following the methodology described in EN 1936:2006 [9]. Six cylindrical specimens with a diameter D and height H were used for these measurements (see Table 1). The selection criteria ensured a surface-to-volume ratio within the range of 0.08 to 0.20 mm^{-1}, making them suitable for the analysis. Prior to testing, specimens were dried at 70 ± 5 °C until a constant mass was achieved.

Each specimen was first weighed in its dry state (dry mass, m_d). Subsequently, the specimens were placed in a vacuum chamber, and the pressure was gradually reduced to 2.0 ± 0.7 kPa. This pressure was maintained for 2 ± 0.2 h to facilitate the removal of air from the open pores of the specimens. After this stage, demineralised water at 20 ± 5 °C was introduced into the chamber at a controlled rate, ensuring that the specimens were completely immersed within at least 15 min. Once all specimens were fully submerged, the chamber was brought back to atmospheric pressure, and the samples remained underwater for 24 ± 2 h.

After the prescribed immersion period, the specimens were weighed while still submerged to record the mass immersed in water (m_h). Then, the specimens were removed from the water and weighed again to determine the saturated mass (m_s). Table 1 shows the results for mass, porosity and density parameters of the six analysed samples.

Table 1. Physical properties of the six analysed samples.

ID Sample	D [mm]	H [mm]	m_d [g]	m_h [g]	m_s [g]	ρ_o [%]	ρ_b [Kg/m^3]
M1	54	56	344.9	217.3	345.4	0.4	2690
M2	54	64	392.1	247.0	392.8	0.4	2680
M3	54	44	280.3	176.7	280.6	0.3	2690
M4	54	41	251.6	158.6	252.0	0.3	2690
M5	54	38	231.3	146.3	232.3	0.4	2690
M6	54	35	217.2	137.2	218.1	0.5	2680
Avg.						0.4	2690
St. Dev.						0.07	5.16
CoV						18.81%	0.19%

Ultrasonic Tests. The Ultrasonic Pulse Velocity (UPV) test is a non-destructive method for assessing the homogeneity of stones by analysing ultrasonic wave propagation. UPV was measured through direct transmission using nine cylindrical samples prepared for uniaxial compressive strength testing, according to the test procedure presented in the EN 12504-4:2005 standard [10]. Variations in wave velocity can indicate differences in density, porosity, and the presence of flaws, such as cracks or voids. Notably, wave velocities are higher when measured parallel to bedding planes and lower when measured perpendicular to them, due to resistance from microfractures and discontinuities in the rock structure. The results shown in Table 2 indicate low anisotropy, with minor fluctuations in velocity ratios implying the rock high compactness.

Table 2. UPV test results

ID Sample	D [mm]	H [mm]	Δt [μs]	v [m/s]	Avg. [m/s]	St. dev. [m/s]	CoV [%]
C1_X	54	136	25.9	5244.89	5462.3	240.31	4.4
C2_X	54	135	24.9	5421.68			
C3_X	54	135	23.6	5720.33			
C1_Y	54	135	23.8	5665.12	5644.69	41.72	0.74
C2_Y	54	135	24.1	5596.69			
C3_Y	54	135	23.9	5672.26			
C1_Z	54	136	23.0	5905.34	5862.54	80.90	1.38
C2_Z	54	135	23.5	5769.23			
C3_Z	54	136	23.0	5913.04			

Dynamic Elastic Modulus. UPV testing estimates the stone dynamic elastic modulus E_d by examining the propagation of elastic waves, which are influenced by the material elastic properties, geometry, and density. The process involves inducing vibrations in a specimen through mechanical excitation and recording its response. This study used two methodologies: (i) flexural excitation with a sensor positioned beneath the sample and (ii) longitudinal excitation, applying the impulse on one end while the sensor was placed on the opposite base. Tables 3 and 4 show the E_d values resulting from the flexural and the longitudinal excitation, respectively.

Table 3. Dynamic Elastic modulus results obtained through flexural excitation.

ID sample	h [mm]	f [Hz]	E_d [MPa]	Avg. [MPa]	St. Dev. [MPa]	CoV [%]
C1X(⊥)	136	10082	70769	67777	2598.15	3.83
C2X(⊥)	135	9852	66476			

(*continued*)

Table 3. (*continued*)

ID sample	h [mm]	f [Hz]	E_d [MPa]	Avg. [MPa]	St. Dev. [MPa]	CoV [%]
C3X(⊥)	135	9811	66087			
C1Y(//)	135	9961	68046	69935	2645.93	3.78
C2Y(//)	135	10315	72959			
C3Y(//)	135	10016	68798			
C1Z(//)	135	10389	75417	72900	3560.41	4.88
C2Z(//)	135	10137	70382			

Table 4. Dynamic Elastic modulus results obtained through longitudinal excitation.

ID sample	h [mm]	f [Hz]	E_d [MPa]	Avg. [MPa]	St. Dev. [MPa]	CoV [%]
C1X(⊥)	136	18150	65564	63377	2182	3.44%
C2X(⊥)	135	17600	61200			
C3X(⊥)	135	17887	63367			
C1Y(//)	135	18376	66794	67231	418.11	0.62%
C2Y(//)	135	18490	67627			
C3Y(//)	135	18442	67274			
C1Z(//)	135	10389	73955	70604	4738.32	6.71%
C2Z(//)	135	10137	67254			

Analyzing the relationship between resonant frequency, apparent bulk density, and dimensions allows for determining the material dynamic elastic modulus E_d, according to the following equation:

$$E_d = 4h^2 f^2 \rho C \tag{1}$$

where h is the length of the specimens, ρ is the average apparent density, f is the resonant frequency, and C is a correction factor that, for cylindrical samples with a free-free boundary condition, is about 1.2 for flexural vibration mode and 1 for longitudinal vibration mode. Tables 3 and 4 show the E_d values resulting from the flexural and the longitudinal excitation, respectively.

3.4 Mechanical Characterization Tests

Static Elastic Properties and Compressive Strength. To obtain compressive strength (f_c) and static elastic modulus (E_s), three specimens (one for each direction, as shown

in Fig. 3a) were tested under uniaxial compression, according to EN 14580:2005 standard [11] and EN 771-6:2011+A1:2015 [12]. The cylindrical samples have a height-to-diameter ratio of 2.5 (H = 135 mm, D = 54 mm), which is necessary to ensure a state of pure compression at the mid-height of the specimen.

For determining E_s, the specimens were tested until they reached 30% of the measured f_c as specified in [11]. Three load cycles were performed, each ranging from 0 to 30% of f_c, as required by the standard [11]. The linear elastic load threshold considered in the cyclic procedure was assessed based on preliminary monotonic tests up to failure. The tests were performed under loading control at a constant stress rate of 0.5 ± 0.2 MPa/s. Three strain gauges, positioned approximately 120° apart, are used to measure vertical strain variations of 5×10^{-3} mm/m (Fig. 6a). Table 5 shows the results of E_s calculated by dividing the stress by the vertical strain variations during the increasing phase of the first load cycle and the stress-strain curves in the three directions.

The compressive strength (f_c) of each specimen was calculated by dividing the maximum load from uniaxial compression tests by the average cross-sectional area (A = 2289.06 mm^2). A total of 19 specimens were tested: 13 cored in the X direction, 3 cored in the Y direction, and 3 cored in the Z direction. The load was applied gradually at a rate of 0.5–1 MPa/s until failure, following the EN 772-1-2011+A1–2015 [12]. Table 6 shows the results of the experimental tests.

Table 5. Static Modulus of Elasticity and stress-strain plot in the 3 directions: X, Y and Z

ID sample	E_s [MPa]
C1X(⊥)	65591
C1Y(//)	62132
C2Z(//)	71284

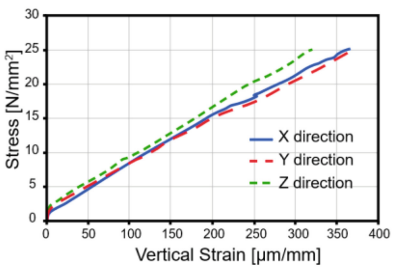

Table 6. Compressive strength for parallel and perpendicular directions

ID sample	Test condition	Max Load [kN]	f_c [Mpa]	Avg. f_c [Mpa]	St. Dev. [Mpa]	CoV [%]
C1X(⊥)	dry	355.09	155.14	149.62	6.29	4.2
C2X(⊥)	dry	342.74	149.72			
C3X(⊥)	dry	309	134.99			
C4X(⊥)	dry	346	151.15			
C5X(⊥)	dry	352	153.77			

(*continued*)

Table 6. (*continued*)

ID sample	Test condition	Max Load [kN]	f_c [Mpa]	Avg. f_c [Mpa]	St. Dev. [Mpa]	CoV [%]
C6X(⊥)	dry	329	143.72			
C7X(⊥)	dry	350	152.90			
C8X(⊥)	dry	348	152.02			
C9X(⊥)	dry	337	147.22			
C10X(⊥)	dry	356	155.52			
C11X(⊥)	sat	358	156.39	157.26	0.76	0.48
C12X(⊥)	sat	361	157.70			
C13X(⊥)	sat	343	157.70			
C1Y(//)	dry	332	145.03	113.82 (143.87)	52.06 (1.64)	45.73 (1.14)
C2Y(//)	dry	123	53.73			
C3Y(//)	dry	327.2	142.71			
C1Z(//)	dry	258	112.71	139.21	45.15	32.43
C2Z(//)	dry	438	191.34			
C3Z(//)	dry	260	113.58			

In the X direction, both specimens in dry (n. 10) and saturated conditions (n.3) were tested. The average compressive strength (f_c) for dry specimens was 149.62 MPa, while for saturated specimens, it was 157.26 MPa. The difference is not significant, proving the stone low porosity. In the Y direction, the average compressive strength is 113.82 MPa. However, it is important to note that specimen C2Y exhibited reduced strength of 53.73 MPa due to an early rupture caused by a naturally sealed microcrack running along the length of the specimen (see Fig. 7a). When excluding this sample, the average compressive strength rises to 143.87 MPa (indicated in brackets in Table 6), which is slightly higher than the average obtained in the Z direction, where it measures 139.21 MPa. Overall, the compressive strength results show that limestone has a very high strength and exhibits low anisotropy. Figure 6 and Fig. 7 show the various failure modes exhibited by specimens in the three different directions X, Y and Z.

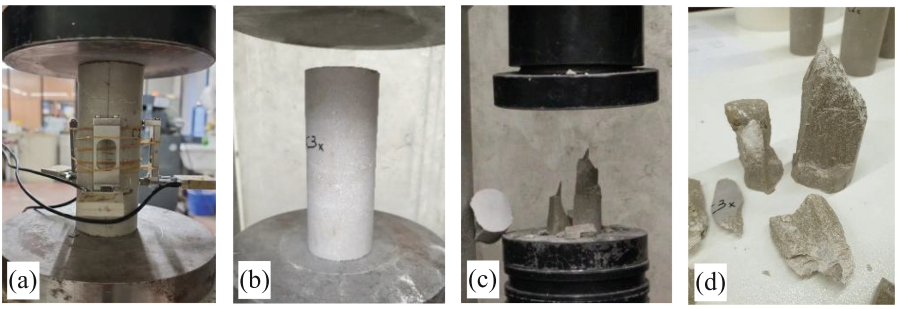

Fig. 6. a) Instrumented specimen; C3X sample before (b) and after (c and d) testing.

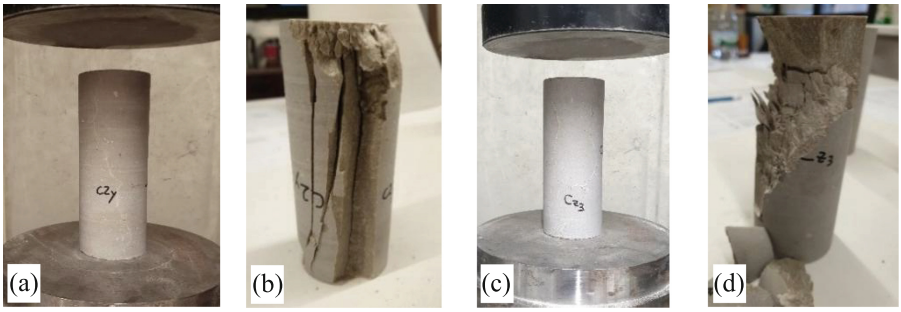

Fig. 7. Failure mode of the samples: a) and b) C2Y; c) and d) C3Z

In general, macroscopic cracks tend to align with the direction of axial loading. However, a clear failure mode cannot be distinctly identified, as the crack patterns are significantly influenced by the material internal structure, particularly the presence of sealed microfractures, which promote progressive failure along weaker planes. For specimens loaded along the X direction, failure appears notably more brittle or explosive compared to the other orientations (Fig. 6). Figure 7a-b shows the crack pattern of a specimen loaded in the Y direction, where, in addition to axial cracks, damage concentration is evident near the loading platens due to stress concentration. Some delaminated portions can also be observed in this region, forming a laminar damage pattern. This laminar failure pattern is more pronounced in the Z direction (Fig. 7c-d), showing inclined, layered fracture surfaces. The rupture isn't purely axial but follows a distinct laminar pattern, likely influenced by the bedding planes. Thin, delaminated slabs indicate weakness along pre-existing stratification planes.

Flexural Strength. Flexural strength was determined by testing specimens according to the EN 12372:2022 standard [13]. Figure 8a illustrates the test setup. A monotonic axial load was applied at the midspan of each specimen at a rate of 0.25 ± 0.05 MPa/s until failure. The maximum load was recorded, and the flexural strength ($f_{tc,f}$) was calculated using the equation:

$$f_{tc,f} = (3Fl)/(2bh^2) \tag{2}$$

where l, b and h are the three dimensions of the specimens. The three tested specimens were initially selected based on the X direction and labelled AX, BX, and CX. They measured 150 × 30 × 30 mm^3, with a tolerance of ±3 mm. They feature a smooth surface finish and were manufactured parallel to the rock bedding plane (X). Table 7 shows the flexural test results. Figure 8 displays the specimens after being tested, showing rupture along a vertical or slightly inclined cracking plane (Fig. 8a) with a low roughness interface (Fig. 8b).

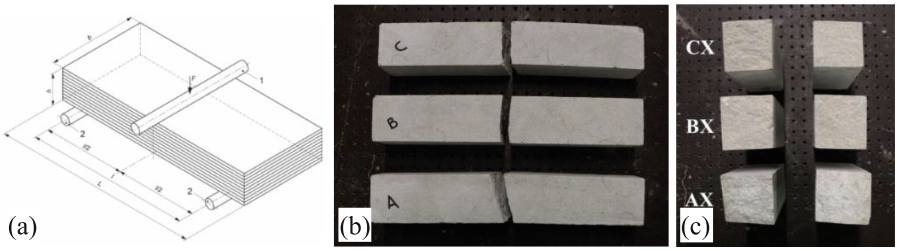

Fig. 8. a) 3-point bending test setup, according to the EN standard. Specimens tested for flexural strength: (b) front view; (c) rupture surface interface.

Table 7. Three-points bending test results.

ID sample	F [KN]	$f_{tc,f}$ [MPa]	Avg. [Mpa]	St. Dev. [Mpa]	CoV [%]
AX	5265	15.80			
BX	6118	18.35	18.60	2.97	16
CX	7239	21.72			

Brazilian Splitting Test. The test is used to determine the indirect tensile strength of cylindrical, cubic, or prismatic specimens. In this case, three prismatic specimens conforming to the standards EN 12350-1 [14], EN 12390-1 [15], and EN 12390-2 [16] were used. The three samples (DX, EX and FX) have a section of 52 × 52 mm^2, with a smooth surface finish and made in a direction parallel to the rock bedding plane (X).

The test involved applying a compressive load to a narrow loading region using cylindrical contact elements. These elements exert the load along a single line until the specimen splits along the prismatic section, which provides an indirect measurement of tensile strength. A constant loading was applied at a rate between 0.04–0.06 MPa/s. Table 8 shows the test results.

It is observed that the higher tensile strength values obtained from 3-point bending tests, compared to those from Brazilian splitting tests, can be attributed to their differing loading conditions, as well as the gradient and distribution of stress. The Brazilian test method creates a uniform tensile stress field across the section and remains unaffected by compressive stresses, in contrast to the 3-point bending test. Because the stone blocks used in masonry composites typically exhibit a failure mode that closely resembles the behaviour observed in Brazilian tests, this method is regarded as a more reliable way to estimate tensile strength.

Table 8. Brazilian splitting test results.

ID sample	F [KN]	$f_{tc,B}$ [MPa]	Avg. [Mpa]	St. Dev. [Mpa]	CoV [%]
DX	37	9.42			
EX	20.22	4.76	6.46	2.57	39.7%
FX	22.16	5.21			

4 Conclusions

This study presents a comprehensive laboratory characterisation of Saltrio stone, obtained from the last active quarry. Saltrio stone is a sedimentary rock with a calcareous composition. It exhibits microfractures and has minimal porosity. The testing also demonstrated the stone high strength, low anisotropy, and compactness.

The research provides valuable data on the physical and mechanical properties of stone blocks, which will aid in the restoration of cultural heritage buildings while maintaining their historical value and integrity. Additionally, properties such as compressive strength and elastic modulus are crucial for assessing the structural integrity and seismic performance of these historical stone masonry structures. Given the lack of recent characterisation in the existing literature, especially in light of new codes, the findings of this study provide valuable insights not only for the conservation of cultural heritage but also for assessing the structural capacity of existing heritage buildings.

Future research will explore the use of Saltrio stone in the construction of full-scale prototypes of stone masonry walls and vaults, which will be tested at the European Laboratory for Structural Assessment (ELSA) at the Joint Research Centre (JRC) in Ispra, Italy. Additional nondestructive tests (e.g. sonic pulse velocity tests, flat jack tests, penetrometric test on mortar) will be employed to evaluate the properties of the masonry, facilitating effective modelling and validation of its structural behaviour.

Acknowledgements. The authors would like to acknowledge Paola Zambelli for her valuable contributions to this research during her master's thesis at Politecnico di Milano. They also acknowledge the Salnova SpA quarry and Mr. Alberto Citrini for their assistance in supplying stone samples for the testing process and the lab technicians of LPMSC for their support in the execution of the tests.

References

1. Baker, D.F., Cassani, R., Sartorelli, P., Galli, B., Trapletti, A.: Le cave di Saltrio, di Brenno e d'oltreoceano. Arti Tipografiche Induno, Induno Olona (Va), Italy (2002) (in Italian)
2. Balzarini, A., Cani, F., Zerboni, A.: Antiche cave nel territorio della Regio Insubrica: Como, Varese, Canton Ticino. Società Archeologica Comense, Como, Italy (2001) (in Italian)
3. Felber, M.: Il Monte San Giorgio. Edizioni Casagrande, Bellinzona, Svizzera (2005) (in Italian)

4. Traversi, G.L., Scesi, L., Arieni, L., Bolognese, M., Mazzucchelli, A.: Le antiche cave sotterranee di Viggù, Saltrio e Brenno: studio geologico, idrogeologico e geologico-tecnico. Geologia Insubrica **10**(1), 1–88 (2007) (in Italian)
5. Bugini, R., Folli, L.: Building Stones of Milan and Lombardy, vol. 2: Stones of Lombardy. CRC Press, Milan (2023) (in Italian)
6. Fiorio, M.T.: Le Chiese di Milano. Electa Editrice, Milano, Italy (1985) (in Italian)
7. Bosellini, A.: Introduzione allo studio delle rocce carbonatiche. Italo Bovolenta editore, Bologna, Italy (1991) (in Italian)
8. Panoramica Palazzo Reale. Wikimedia Commons. Available at: URL (License: CC BY-SA 4.0)
9. EN 1936:2006 Natural stone test methods—Determination of real density and apparent density, and of total and open porosity
10. EN 12504-4:2005 Testing concrete – Determination of ultrasonic pulse velocity
11. EN 14580:2005, Natural stone methods – Determination of static elastic modulus
12. EN 771-6:2011+A1:2015 Specifications for masonry units – Natural stone masonry units
13. EN 12372:2022 Natural stone test methods - Determination of flexural strength under concentrated load
14. EN 12350-1 Testing fresh concrete – Part 1: sampling and common apparatus
15. EN 12390-1 Testing hardened concrete - Shape, dimensions and other requirements for specimens and moulds
16. EN 12390-2 Testing hardened concrete - Part 2: Making and curing specimens for strength tests